Bone Reports 11 (2019) 100218

Contents lists available at ScienceDirect

Bone Reports

journal homepage: www.elsevier.com/locate/bonr

Stat3 in osteocytes mediates osteogenic response to loading

Kylie A. Corry[a,1], Hongkang Zhou[a,1,2], Tatiana Brustovetsky[b], Evan R. Himes[a], Nicoletta Bivi[c,3], M. Ryne Horn[d], Yukiko Kitase[c], Joseph M. Wallace[d], Teresita Bellido[c,e], Nickolay Brustovetsky[b], Jiliang Li[a,*]

[a] Department of Biology, Indiana University Purdue University Indianapolis, Indianapolis, IN 46202, USA
[b] Department of Pharmacology and Toxicology, Indiana University School of Medicine, Indianapolis, IN 46202, USA
[c] Department of Anatomy and Cell Biology, Indiana University School of Medicine, Indianapolis, IN 46202, USA
[d] Department of Biomedical Engineering, Indiana University Purdue University Indianapolis, Indianapolis, IN 46202, USA
[e] Roudebush Veterans Administration Medical Center

ARTICLE INFO

Keywords:
Signal transducers and activators of transcription 3 (Stat3)
Mechanotransduction
Osteocyte
ROS
ATP
Bone formation

ABSTRACT

Signal transducer and activator of transcription 3 (Stat3) is a member of the Stat family of proteins involved in signaling in many different cell types, including osteocytes. Osteocytes are considered major mechanosensing cells in bone due to their intricate dendritic networks able to sense changes in physical force and to orchestrate the response of osteoclasts and osteoblasts. We examined the role of Stat3 in osteocytes by generating mice lacking Stat3 in these cells using the Dmp-1(8kb)-Cre promoter (Stat3cKO mice). Compared to age-matched littermate controls, Stat3cKO mice of either sex (18 weeks old) exhibit reduced bone formation indices, decreased osteoblasts and increased osteoclasts, and altered material properties, without detectable changes in bone mineral density (BMD) or content of either trabecular or cortical bone. In addition, Stat3cKO mice of either sex show significantly decreased load-induced bone formation. Furthermore, pharmacologic inhibition of Stat3 in osteocytes *in vitro* with WP1066 blocked the increase in cytosolic calcium induced by ATP, a mediator of the cellular responses to sheer stress. WP1066 also increased reactive oxygen species (ROS) production in cultured MLO-Y4 osteocytes. These data demonstrate that Stat3 is a critical mediator of mechanical signals received by osteocytes and suggest that osteocytic Stat3 is a potential therapeutic target to stimulate bone anabolism.

1. Introduction

Signal transducer and activator of transcription 3 (Stat3) is a globally expressed transcription factor located in the cytoplasm that can be activated by cytokines, including members of the IL-6 family (IL-6, IL-11, oncostatin M, leukemia inhibitory factor, cardiotrophin 1, and neurotrophin1/B-cell stimulatory factor 3) (Heinrich et al., 1998; Senaldi et al., 1999; Aaronson and Horvath, 2002; Levy and Lee, 2002; Levy and Loomis, 2007). Mutations in the STAT3 gene cause a rare immunodeficiency disease called Job's Syndrome, also known as Hyperimmunoglobulin E syndrome (Holland et al., 2007; Minegishi et al., 2007). Affected patients have elevated levels of IgE in their serum and have craniofacial abnormalities. (Freeman and Holland, 2008) These patients also present other skeletal abnormalities, such as reduced bone mineral density (BMD) and recurrent fractures (Sowerwine et al., 2014). Recent studies including our own suggest that Stat3 affects mitochondrial activity and Stat3 deficiency leads to increased levels of ROS in osteoblasts (Gough et al., 2009; Wegrzyn et al., 2009; Boengler et al., 2010; Sarafian et al., 2010; Zhou et al., 2011). In earlier studies, we generated conditional Stat3 knockout (KO) mice in which Stat3 was deleted in both osteoblasts and osteocytes (with type I collagen promoter driven Cre deletor) and found that they exhibited lower BMD and reduced bone strength (Zhou et al., 2011). However, because Stat3 was deleted from both osteoblasts and osteocytes, it was not possible to differentiate the role of Stat3 in each cell type.

Osteocytes are found embedded in bone and make up a complex network of dendritic processes, and therefore are considered to be the most important mechanosensing cells in bone (Rubin, 1984; Turner

* Corresponding author at: Department of Biology, Indiana University Purdue University Indianapolis, 723 W Michigan Street, SL306, Indianapolis, IN 46202, USA.
E-mail address: jilili@iupui.edu (J. Li).
[1] These authors contributed equally to this work.
[2] Current affiliation: Department of Anatomy and Neurobiology, School of Basic Medical Science, Central South University, Changsha, Hunan Province 410013, P. R. China.
[3] Current affiliation: Lilly Research laboratories, Eli Lilly and Company, Indianapolis, IN, USA.

https://doi.org/10.1016/j.bonr.2019.100218
Received 9 July 2019; Accepted 26 July 2019
Available online 29 July 2019

et al., 1994; Robling et al., 2002). Stat3 is known to be one of the early response genes up-regulated upon mechanical loading (Mantila Roosa et al., 2011). In the current study, we generated mice in which Stat3 was deleted from osteocytes by using mice in which the Cre deletor was under the control of the dentin matrix protein 1 (Dmp1-8kb-Cre) promoter, which targets genes primarily to osteocytes in bone (Bivi et al., 2012). Using these osteocytic Stat3 KO mice, we investigated its role in these cells and particularly in mechanotransduction. We further examined the role of Stat3 signaling in the osteocytic cell line MLO-Y4. We found that bone apposition in response to mechanical loading is defective in Stat3cKO mice and that a pharmacologic Stat3 inhibitor increases ROS in MLO-Y4 cells and inhibits an increase of the intracellular calcium concentration induced by external ATP, a recognized mediator released by mechanical stimulation. We conclude that Stat3 is an essential component of the machinery activated by mechanical forces in osteocytes.

2. Materials and methods

2.1. Experimental animals

All procedures in this study were in accordance with the Indiana University Purdue University Indianapolis (IUPUI) School of Science Animal Care and Use Committee Guidelines. The transgenic mice expressing Cre in osteocytes (Dmp1-Cre) under the control of the dentin matrix protein 1 promoter (8 kb) were generated and characterized, as previously described (Bivi et al., 2012). The $Stat3^{flox/flox}$ mice with exons 18-20 of the Stat3 gene flanked by LoxP sites were created and generously provided by Dr. Xin-Yuan Fu (Department of Biochemistry, National University of Singapore, Yong Loo Lin School of Medicine) (Welte et al., 2003). Exons 18-20 of the Stat3 gene encode the SH2 domain of the protein which is required for Stat3 activation. Conditional osteocyte-specific Stat3 KO (Stat3cKO) mice were generated by breeding mice containing the Cre recombinase driven by the Dmp-1 promoter with mice with floxed Stat3. Three distinct genotypes of mice were generated for experiments: Dmp1-Cre; $Stat3^{flox/flox}$ (Stat3cKO) for experimental mice; $Stat3^{flox/+}$ for breeding, and Dmp1-Cre; $Stat3^{+/+}$ as the wild-type littermate controls. Genotype of the mice was confirmed using polymerase chain reaction. Stat3 forward primer 5⊕-ATTGGA ACCTGGGACCAAGTGG-3⊕ and reverse primer 5⊕-ACATGTACTTA CAGGGTGTGTGC-3⊕ were used for amplifying the LoxP site. The PCR for detecting the DNA sequence of the LoxP site amplified a 520 bp DNA band for $Stat3^{flox/flox}$ and a 480 bp DNA band for $Stat3^{+/+}$, while the PCR for the heterozygous Stat3 floxed mice ($Stat3^{flox/+}$) amplified both 520 bp and 480 bp bands (Welte et al., 2003). The PCR for Stat3cKO mice amplified a floxed Stat3 band of 520 bp and a 615 bp Cre band, whereas, for the littermate control mice, PCR amplified a 490 bp Stat3 band and a 615 bp Cre band.

2.2. In vivo ulna loading

Dynamic axial ulna loading was performed on 16-week-old, Stat3cKO mice and their littermate controls under general anesthesia using 3–5% isoflurane (Sigma-Aldrich, St. Louis, MO, USA) (Zhou et al., 2011). The right ulnae were loaded for 120 cycles/day at a frequency of 2 Hz with a peak force of 2.5 N for female mice and 2.8 N for male mice. This same loading procedure was performed for 3 consecutive days using an electromagnetic actuator (TA ElectroForce 3200 series, Castle, DE). The loading forces were selected based on a pilot load-strain calibration using 3 randomly selected mice from each gender and genotype. The peak force of 2.5 N in females and 2.8 N in males produced about ~2800 and ~2900 microstrain at the midshaft of ulnas in control and conditional Stat3 KO mice, respectively. Mechanical strains experienced during loading were determined using a strain gauge on the medial surface of the ulnae as described previously by our lab (Li et al., 2005; Zhou et al., 2011). The left ulnae served as non-loaded internal controls. All mice were allowed normal cage activity between and after each loading session, and were given food and water ad libitum. An intraperitoneal injection of calcein (green fluorochrome label, 30 mg/kg body weight, Sigma-Aldrich) was administered on day 5 after the first loading session. Then, another fluorescent dye, alizarin (red fluorochrome label, 50 mg/kg body weight, Sigma-Aldrich), was administered on the 11th day after the first loading session, making the inter-label time 6 days. The mice were euthanized 14 days after loading and a series of bone specimens were collected (ulnae, radii, femurs, tibiae, and the vertebrae) for further analysis, including histomorphometry.

2.3. Histomorphometry

Histomorphometry was performed on both the 18-week-old Stat3cKO mice and their littermate controls. The bone specimens were fixed in 10% neutral buffered formalin for 24 h, then dehydrated through a series of graded alcohols, cleared in xylene, and then embedded in liquid methyl methacrylate. Using a diamond-embedded wire saw (Histo-saw; Delaware Diamond Knives, Wilmington, DE), transverse thick sections (70 μm) were cut at the ulnar midshafts, ground to a final thickness of 20 μm, and mounted on microscope slides. Three sections per limb were used for bone histomorphometry with a Nikon Optiphot fluorescence microscope (Nikon, Inc., Garden City, NJ) using a Bioquant digitizing system (R&M Biometrics, Nashville, TN). The following primary data were collected from the periosteal surface at 250Ô magnification: total perimeter (B.Pm); single label perimeter (sL.Pm); double label perimeter (dL.Pm); and double label area (dL.Ar). From these primary data, the following quantities were derived: mineralizing surface (MS/BS = [1/2sL.Pm + dL.Pm] / B.Pm Ô 100; %); mineral apposition rate (MAR = dL.Ar/dL.Pm/6 days; μm/day); and bone formation rate (BFR/BS = MAR Ô MS/BS Ô 3.65; $\mu m^3/\mu m^2$ per year). Furthermore, a set of relative (r) values such as rMS/BS, rMAR, and rBFR/BS were calculated by subtracting the values for the left ulna (non-loaded) from the values for the right ulna (loaded).

From the distal femurs and lumbar vertebral bodies (L4), 5-μm-thick frontal sections were cut using a microtome (Leica, Germany). For each set of the bone sections from femurs and vertebrae, two unstained sections were mounted on microscope slides, while other sections were stained with tartrate-resistant acid phosphatase (TRAP) to identify active osteoclasts. The following primary data were collected from the metaphyseal area, 0.5 mm distal to the growth plate and 0.5 mm away from the intracortical surface, at 250Ô magnification: tissue area (T.Ar), trabecular bone area (tB.Ar), trabecular bone perimeter (tB.Pm), single label perimeter (sL.Pm), double label perimeter (dL.Pm), double label area (dL.Ar), osteoclast surface (Oc.S), and osteoclast number (Oc.N). From these primary data, the following quantities were derived: bone volume (BV/TV = tB.Ar/T.Ar Ô 100; %), mineralizing surface (MS/BS = [1/2sL.Pm + dL.Pm]/B.Pm Ô 100; %), mineral apposition rate (MAR = dL.Ar/dL.Pm/6 days; μm/day), bone formation rate (BFR/BS = MAR Ô MS/BS Ô 3.65; $\mu m^3/\mu m^2$ per year), percentage of osteoclast surface (Oc.S/BS = Oc·S/tB·Pm; %), and osteoclast number per mm (Oc.N/BS = Oc.N/tB.Pm; #/mm).

2.4. Micro-computed tomography (μCT)

The μCT was performed on the left femurs from 18-week-old WT and osteocyte-specific Stat3 KO mice. Femurs were brought to room temperature and scanned using μCT (SkyScan 1172, Bruker-microCT, Kontich, Belgium) using the scanning parameters as follows: Voltage: 60 kV, Resolution: 6 μm, Binning mode: 2 K, Filter: Al 0.5 mm, Rotation step: 0.7°, and Averaging frame: 2. Once scanned, the raw images were reconstructed using SkyScan NRecon software (Bruker-microCT, Kontich, Belgium). Analysis of the μCT 3-D data was then performed using SkyScan CT-Analyser (CTAn) (Bruker-microCT, Kontich, Belgium). A thickness of 1 mm of trabecular bone 0.5 mm proximal to

the distal growth plate was used to analyze the trabecular bone while cortical bone analysis was conducted at the midshaft.

2.5. Peripheral dual-energy X-ray absorptionmetry (pixiMUS)

Bone mineral content (BMC, g) and bone mineral density (BMD, g/mm^2) of the left femurs were evaluated using peripheral dual-energy X-ray absorptiometry (pDXA; PIXIMus II; GE-Lunar Co.).

2.6. Biomechanical testing

Three-point bending was performed on the same left femurs after μCT. Femurs were slowly brought to room temperature and remained fully hydrated throughout testing. A span was set based on the shortest femur at 6.84 mm, with the top point at the midpoint (3.42 mm). Each femur was loaded into a 500 lb. actuator with a 25 lb. load cell (TestResources Inc., Shakopee, MN 55379, USA), anterior side upward and the distal end to the right. The loading was performed at a rate of 0.03 mm/s until failure. Force-displacement data were collected at a frequency of 25 Hz and used to generate a force-displacement curve where structural strength, stiffness, deformation, and work were calculated using a custom Matlab script. (Robinson et al., 2006; Berman et al., 2016; Hammond et al., 2016) The μCT data at the fracture site were then used to calculate estimated material properties, including stress, strain, Young's modulus, and total toughness using beam bending theory.

2.7. Calcium imaging

Calcium imaging, adopted from our previous methods using neurons in culture (Pellman et al., 2015), was performed to measure the cytosolic Ca^{2+} concentration ($[Ca^{2+}]_c$) in cultured MLO-Y4 osteocyte-like cells and MC3T3-E1 osteoblasts. MLO-Y4 osteocytes and MC3T3-E1 osteoblasts were cultured in μ-slide I Leur (Ibidi GmbH, Germany) overnight before shear stress was applied or ATP was used as the treatment. To follow changes in $[Ca^{2+}]_c$, osteocytes were loaded at 37 °C with 2.6 μM Fura-2AM (Molecular Probes, Eugene, OR) in the standard bath solution containing 139 mM NaCl, 3 mM KCl, 0.8 mM $MgCl_2$, 1.8 mM $CaCl_2$, 10 mM NaHEPES, pH 7.4, 5 mM glucose, and 15 mM sucrose. Sucrose was used to maintain osmolarity similar to that in the growth medium (300 mOsm). Osmolarity of the bath solution was measured with an osmometer, Osmette II≻ (Precision Systems Inc., Natick, MA). Fura-2 fluorescence signals were measured with a Nikon Eclipse TE2000-U inverted microscope equipped with a Nikon CFI S Fluor 20 Ô 0.75 NA objective and a Photometrics cooled CCD camera CoolSNAP$_{HQ}$ (Roper Scientific, Tucson, AZ) controlled by MetaFluor 6.3 software (Molecular Devices, Downingtown, PA). The excitation light was delivered by a Lambda-LS system (Sutter Instruments, Novato, CA). The excitation filters (340 ± 5 and 380 ± 7 nm) were controlled by a Lambda 10-2 optical filter changer (Sutter Instruments, Novato, CA). Fluorescence was recorded through a 505 nm dichroic mirror at 535 ± 25 nm. The images were taken every 15 s during the time-course of the experiment using the minimal exposure time that provided acceptable image quality. The changes in $[Ca^{2+}]_c$ were monitored by following a ratio of F_{340}/F_{380}, calculated after subtracting the background from both channels. $[Ca^{2+}]_c$ was calculated using the Grynkiewicz method (Grynkiewicz et al., 1985), assuming K_d for Fura-2 is 0.224 μM. Since Ca^{2+} binding and spectroscopic properties of fluorescent dyes can differ significantly in the intracellular milieu, the cytosolic Ca^{2+} concentrations presented in this paper should be deemed estimates as stated previously by other investigators (Dietz et al., 2007; Stanika et al., 2009).

2.8. ROS production

The rate of ROS production in MLO-Y4 osteocyte-like cells was evaluated by measuring fluorescence of dihydroethidium (DHE) (Vergun et al., 2001) employing the same setup used for calcium imaging. DHE (5 μM) was present in the bath solution during the experiment with osteocytes. DHE was excited at 545 nm, and emission was recorded at 620 nm.

2.9. Statistical analysis

The data are expressed as mean ± SEM (standard error of the mean). Data of the *in vivo* experiments were analyzed by a two-way ANOVA to test for differences among the Stat3cKO and WT groups comparing males and females. None of the parameters measured showed a statistically significant interaction; therefore, interaction p values are not reported. The data of the *in vitro* experiments were analyzed by t-test. Statistical significance was assumed for $p < 0.05$.

3. Results

To assess the successful elimination of Stat3 from osteocytes, immunohistochemistry was performed to probe for the presence of Stat3 proteins. Stat3 proteins were found in the osteocytes of the wild type mice, but not in the osteocytes of the conditional Stat3 KO mice (Figs. 1: A1 & B1).

Stat3cKO mice, either male or female, exhibited growth rates undistinguishable from WT littermate controls and no differences in body weight, BMC, or BMD were observed. Data corresponding to 18 weeks of age are shown in Supplemental Table S1. In addition, trabecular bone volume showed no significant difference at the distal femur (Figs. 1: A2 & B2 and 2). However, the osteoid surface of trabecular bone (OS/BS) was significantly decreased in the Stat3cKO compared to WT littermate controls (Fig. 2). Male Stat3cKO mice were 46.2% lower than the male controls ($p < 0.05$), and in females the osteoid surface of the Stat3cKO mice was 75.8% lower than the female controls ($p < 0.01$) (Fig. 2). Compared to WT control mice, in females, the mineralizing surface (MS/BS) of the Stat3cKO mice was reduced by 30% ($p < 0.05$), and in males, the MS/BS of the Stat3cKO mice was 35.3% ($p < 0.01$) lower (Fig. 2). In the females, the mineral appositional rate (MAR) of the Stat3cKO mice was 41% ($p < 0.01$) lower, and in the males, the MAR of the Stat3cKO mice was 35.6% ($p < 0.01$) lower (Fig. 2). Finally, the bone formation rate (BFR/BS) of the Stat3cKO mice was 58.1% ($p < 0.01$) and 57.8% ($p < 0.01$) lower in the females and the males, respectively (Fig. 2). Decrease in bone formation related parameters were also observed at the midshafts of femurs (Supplemental Fig. S1). Overall, Stat3 deficiency in osteocytes does not affect bone mineral accrual, but suppresses bone formation in adult mice.

TRAP staining was performed to assess the number of osteoclasts present and measure the amount of osteoclast surface. The osteoclast number (N.Oc/B.Pm) in the conditional Stat3 KO mice was significantly greater than that of the WT mice (Fig. 3). Compared to their WT controls, in females, N.Oc/B.Pm of the Stat3cKO mice were 104% greater ($p < 0.01$), and in males, N.Oc/B.Pm of Stat3cKO mice were 146% greater ($p < 0.01$) (Fig. 3). The osteoclast surface (Oc.S/BS) of the conditional Stat3 KO mice was also significantly greater than that of their WT littermate controls. Compared to WT controls, in females, Oc.S/BS of the Stat3cKO mice was 110% greater ($p < 0.01$), and in males, Oc.S/BS of Stat3cKO mice was 177% greater ($p < 0.01$) (Fig. 3). Overall, these results indicate an increased osteoclast number in the conditional Stat3 KO mice.

Mechanical testing of the femur in three-point bending revealed no difference in structural mechanical properties of femurs between the Stat3 cKO and WT littermate controls (Fig. 4). Further analysis based on diaphyseal geometry (Table 1) revealed significant differences in estimated bone material properties between the Stat3 cKO and WT control mice. Compared to WT control mice, the ultimate stress of the Stat3 cKO mice was 19.6% ($p < 0.01$) lower in males, the ultimate stress of the Stat3 cKO mice was 18.8% ($p < 0.001$) lower in females (Fig. 4).

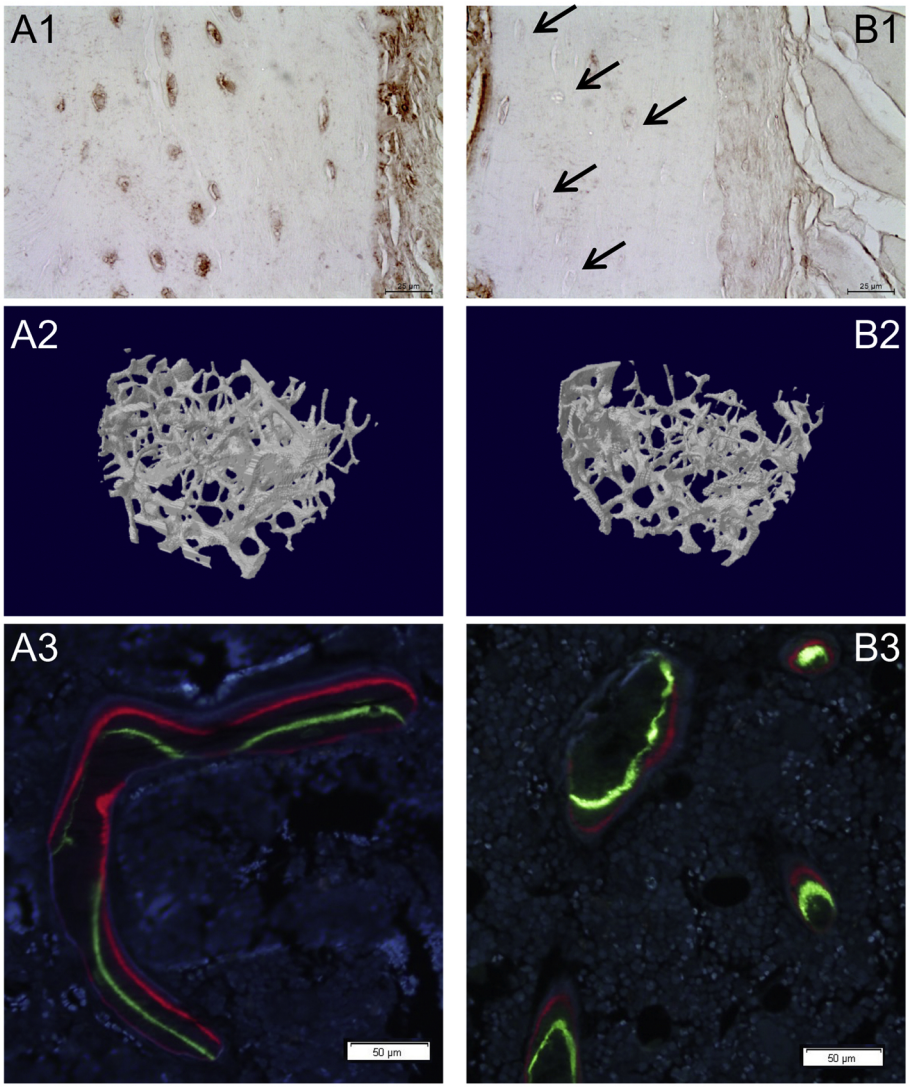

Fig. 1. Osteocytes specific Stat3 knockout leads to decreased Stat3 protein expression in osteocytes and lower bone mass compared to WT mice.
Immunohistochemical staining of experimental mice cortical bone of femurs. Immunohistochemical staining demonstrates the expression of Stat3 protein in 8-week-old osteocytes of the Dmp1-Cre; $Stat3^{+/+}$ (WT control) mouse (A1). Stat3 proteins in osteocytes were stained brown and dark brown. However, there was no Stat3 protein expression in osteocytes of the Dmp1-Cre; $Stat3^{flox/flox}$ (conditional Stat3 KO) mouse (B1). Black arrows indicate osteocytes without Stat3 proteins probed by brown stains in conditional Stat3 KO mouse (Scale bar = 25 μm). Three-dimensional images of distal femur trabecular bones show, compared to Dmp1-Cre;$Stat3^{+/+}$ (WT) mouse trabecular bones (A2), the Dmp1-Cre;$Stat3^{flox/flox}$ (KO) mouse trabecular bones (B2) demonstrated no significant difference in trabecular bone number and volume. Trabecular bone in the distal femur with fluorescent labels (calcein and alizarin) in (A3) Dmp1-Cre;$Stat3^{+/+}$ (WT) and (B3) Dmp1-Cre;$Stat3^{flox/flox}$ (KO) mice, indicating less labels in conditional Stat3 KO mice.

The same trends were noted for Young's modulus which was 32.3% ($p < 0.05$) lower in male Stat3 cKO mice, and 16.6% ($p < 0.01$) lower in female Stat3 cKO mice compared to sex-matched WT mice (Fig. 4).

Moreover, ulnar loading mice revealed that load-induced bone formation was suppressed in both the male and female osteocyte-specific Stat3 KO mice as quantified by dynamic histomorphometry. Thus, compared to their WT littermate controls, the relative mineralizing surface (rMS/BS), the relative mineral appositional rate (rMAR), and the relative bone formation rate (rBFR/BS) in response to axial ulna loading were all significantly lower in the Stat3 cKO mice. rMS/BS was significantly lower in Stat3 cKO mice (↙49% in male, $p < 0.001$ and –56% in female, $p < 0.001$) than their WT littermate controls (Fig. 5). rMAR was significantly lower in the Stat3 cKO mice (↙66% in male, $p < 0.001$ and –69% in female, $p < 0.001$) than their WT littermate controls (Fig. 5). rBFR/BS was significantly lower in Stat3 cKO mice (↙76% in male, $p < 0.001$ and –77% in female, $p < 0.001$) than their WT littermate controls (Fig. 5).

In order to examine the role of Stat3 in mechanotransduction at the cellular level, we applied fluid shear stress on cultured MLO-Y4 osteocyte-like cells. The shear stress imposed over bone cells caused transient increases in $[Ca^{2+}]_c$ (Supplemental Fig. S2). Fig. 6A shows a representative bright field image of osteocytes in culture. Fig. 6B shows a pseudocolored image of cultured osteocytes loaded with Fura-2AM and subjected to shear stress, whereas Fig. 6C shows changes in $[Ca^{2+}]_c$ in cultured osteocytes subjected to shear stress. Here and in other similar figures, black traces represent signals from individual cells, whereas red trace shows an averaged signals ± SEM.

Previously, it has been shown that the increase in $[Ca^{2+}]_c$ caused by the shear stress is due to release of ATP and stimulation of purine receptors (You et al., 2002; Chen et al., 2003; Genetos et al., 2005; Genetos et al., 2007). Here, we tested whether Stat3 affected the Ca/ATP signaling induced by mechanical stimulation of osteocytic cells *in vitro*. We examined the effect of external ATP on $[Ca^{2+}]_c$ in cultured osteocytes (Fig. 6A) in comparison with osteoblasts (Fig. 6B). While 1 μM ATP fails to stimulate Ca^{2+} influx in both osteocytes and osteoblasts, 100 μM ATP can significantly increase $[Ca^{2+}]_c$ in both osteocytes and osteoblasts. Interestingly, 10 μM ATP significantly increases Ca^{2+} transients in osteocytes, but fails to do so in osteoblasts, suggesting osteocytes are more sensitive to ATP treatment than osteoblasts. The repeated exposures to 10 μM ATP produced uniform Ca^{2+} transients in osteocytes (Fig. 6C). When mitochondria were depolarized by FCCP (10 μM), a protonophore that uncouples oxidative phosphorylation, (Luvisetto et al., 1987) ATP-induced Ca spikes were gradually suppressed despite that the first spike remained unaffected (Fig. 6D). These data indicated FCCP didn't increase cytosolic Ca^{2+}, suggesting that mitochondria were not the major Ca storage in osteocytes. Further, although the first Ca^{2+} transient in osteoblasts following ATP application was not depended on external Ca^{2+}, the subsequent responses to ATP significantly subsided and finally disappeared (Fig. 6E). The similar effect was produced by thapsigargin (Fig. 6F), an inhibitor of

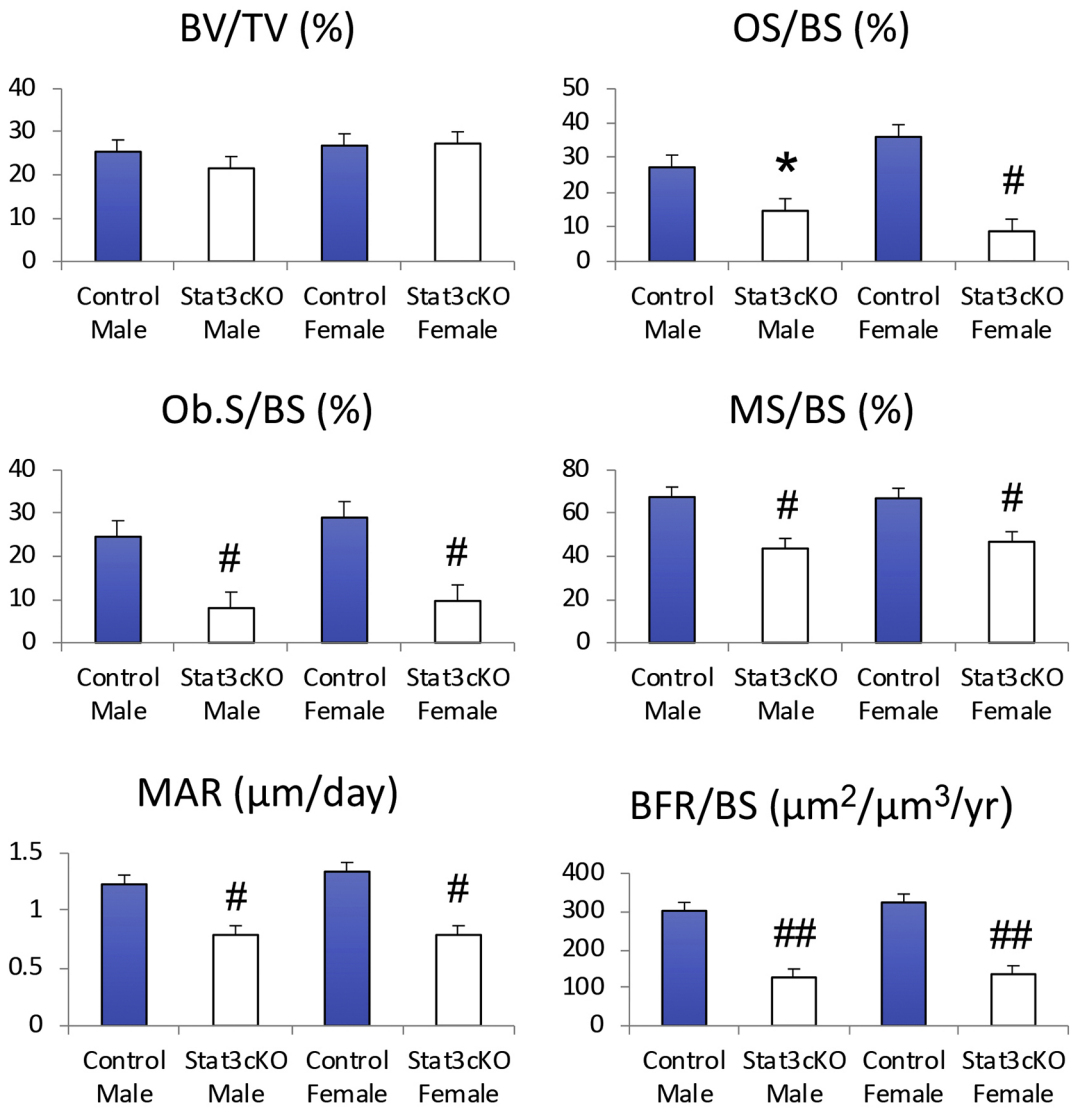

Fig. 2. Stat3 cKO mice exhibit lower BV/TV and decreased bone formation.
Histomorphometric measurements of trabecular bone in the distal femur indicate bone volume (BV/TV), Osteoid surface (OS/BS), Osteoblast surface (Ob.S./BS), mineralizing surface (MS/BS), mineral appositional rate (MAR) and bone formation rate (BFR/BS). Note that *: $p < 0.05$, #: $p < 0.01$ and ##: $p < 0.001$ versus the same sex control.

Ca^{2+}-ATPase in endoplasmic reticulum (ER).(Thastrup et al., 1990) These data suggest that external ATP induces Ca^{2+} release from ER that depletes ER Ca^{2+} storage and requires ER refilling for subsequent Ca^{2+} releases and, therefore, depends on external Ca^{2+}.

The repeated exposures to 10 µM ATP produced uniform Ca^{2+} transients in osteocytes (Fig. 7A). However, Ca^{2+} transients in osteocytes triggered by ATP are inhibited by WP1066, an inhibitor of Stat3 (Iwamaru et al., 2007) (Fig. 7B). Further, in comparison to the vehicle control (Fig. 7C), WP1066 significantly stimulated ROS production in osteocytes (Fig. 7D).

4. Discussion

This study shows that Stat3 KO specific for osteocytes does not affect bone mineral accrual. However, in adult mice, Stat3 deficiency in osteocytes slows down bone formation rate and decreases bone material properties. More importantly, Stat3 deletion specifically in osteocytes suppresses load-driven bone formation markedly in comparison with the littermate controls. ATP induces an increase in $[Ca^{2+}]_c$ in osteocytes. However, Stat3 inhibitor blocks ATP-induced elevation in $[Ca^{2+}]_c$. These data suggest Stat3 plays an important role in osteocytes and in mechanotransduction in adult mice.

At the tissue level, we observed significantly decreased osteoid surface in the 18-week-old KO mice. Though the content of the bones was normal, lack of Stat3 in the osteocytes might be affecting the bone's ability to initiate new bone formation via the transduction of mechanical signals. These data suggest Stat3 deficiency did not affect bone accrual during skeletal development because Stat3 in osteoblasts was intact. Once the mice reach adult ages, the role of osteocytes in bone homeostasis becomes dominant. These deficits in new bone formation were observed in both the midshaft femoral periosteum and the trabecular bone of the distal femurs. A closer look at the osteoclast activity via TRAP staining showed that osteoclast number, osteoclast surface, and the amount of eroded bone surface of the KO mice was significantly greater. Moreover, there was significantly larger bone marrow area and an increase in periosteal perimeter of the femoral midshaft in the osteocyte-specific Stat3 KO mice. These data suggest that the bone modeling process was pushed towards creating more outward growth in the Stat3 cKO mice. The increase in bone resorption on the endosteal surface by osteoclastic activity resulted in an increase in bone marrow

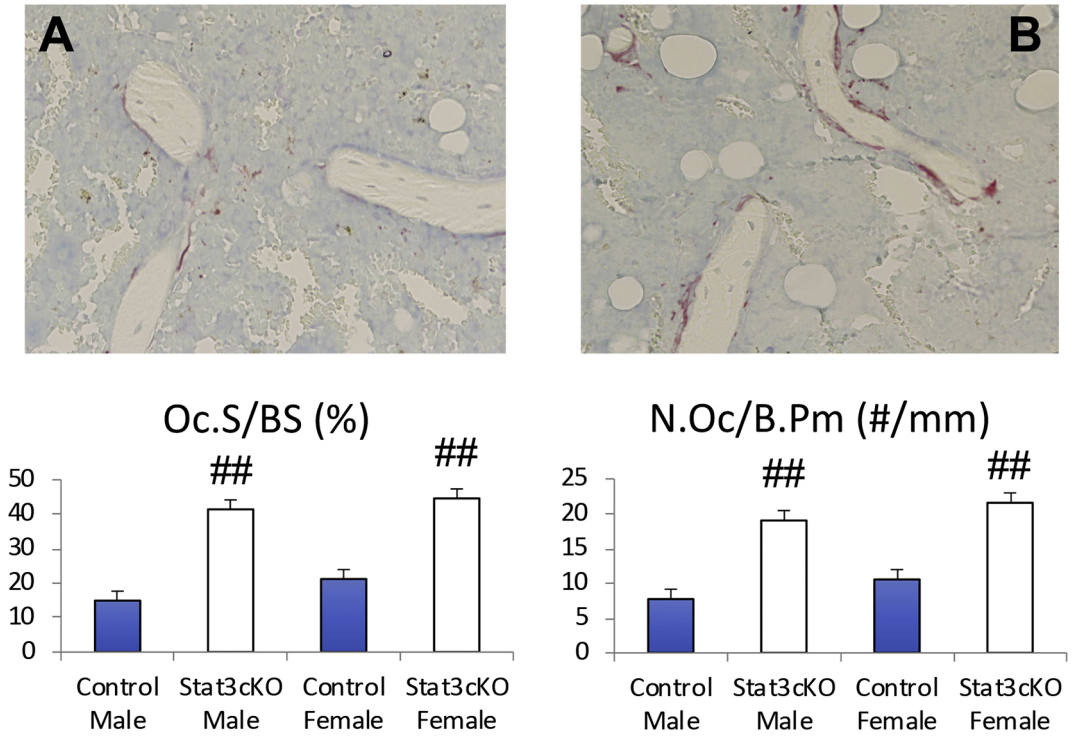

Fig. 3. Stat3 cKO mice exhibit higher bone resorption than the WT control. TRAP stained osteoclasts on trabecular bone surfaces in distal femurs. Compared to Dmp1-Cre;Stat3$^{+/+}$ (WT) mouse (A), Dmp1-Cre;Stat3$^{flox/flox}$ (KO) mouse (B) presented more osteoclast number and osteoclast surface (red stain on trabecular bone surface) on trabecular bone in the similar region of distal femur 0.5 mm above the growth plate. Scale bar = 50 μm.
Osteoclast surface (Oc.S/BS) of osteocyte-specific Stat3 KO mice were 177% greater in males and 110% greater in females compared to their controls. Osteoclast number (N.Oc/B.Pm) of osteocyte-specific Stat3 KO mice were 146% greater in males and 104% greater in females compared to their controls.

area for the Stat3 cKO mice. The coordinated action of osteoclasts on the endosteal surface and the osteoblastic activity on the periosteal surface led to a greater midshaft femoral perimeter in the Stat3 cKO mice.

Analysis of the bone mechanical properties of the Stat3 cKO mice showed significant deficiencies. Deletion of Stat3 in osteocytes decreased the bone material properties. However, the structural properties of the KO mice were normal. These data suggest that the larger bone size compensates for and normalizes the structural mechanical properties of the bone. How Stat3 in osteocytes affects bone material properties remains to be investigated.

Mechanical loading stimulates osteoblasts and osteocytes to produce IL-6 and IL-11 (Kido, Kuriwaka-Kido et al., 2009, Sanchez et al., 2009, Bakker et al., 2014), which in turn act on osteocytes to activate Stat3 via IL-6 receptors. These data indicate that IL-6 cytokines and its receptors mediate Stat3 activation in response to mechanical loading, suggesting a critical role of Stat3 in mechanotransduction. In this study, the ulna loading study revealed significantly reduced load-induced bone formation in the conditional Stat3 KO mice compared to the WT mice. Stat3 is a critical signal transducer and seems to play a pivotal role in the signaling that takes place after mechanical loading. Inactivation of Stat3 in the osteocytes of mice strongly reduces this mechanical signal transduction, leading to a decrease in load-induced bone formation. An increase in the level of ROS in Stat3 deficient osteocytes may suppress osteocyte sensitivity to loading. ROS is a known inhibitor of bone formation, which works by antagonizing normal Wnt signaling (Almeida et al., 2007). The involvement of Stat3 as a regulator of ROS in osteocytes is a potentially novel mechanism that requires further research.

Another mechanism by which Stat3 affects mechanosensitivity of osteocytes is related to ATP-induced increases in $[Ca^{2+}]_c$. It is known that mechanical stimulation induces an immediate release of ATP (Genetos et al., 2005; Genetos et al., 2007), indicating that ATP is an acute mediator at the very early phase of mechanotransduction. The data in the present study show that ATP increases $[Ca^{2+}]_c$ in both osteoblasts and osteocytes. More importantly, ATP concentration necessary to increase $[Ca^{2+}]_c$ in osteocytes is 10-fold lower than the one needed in osteoblasts. These data suggest that osteocytes are more sensitive to extracellular ATP than osteoblasts, consistent with the concept that osteocytes are more sensitive to mechanical stress than osteoblasts. The initial augmentation of Ca spike in the presence of thapsigargin most likely was due to inability of ER Ca-ATPase to remove Ca from the cytosol. An inhibition of Ca responses to subsequent ATP treatments in the presence of thapsigargin was due to a failure of ER Ca-ATPase to replenish Ca storage in ER. The suppression of Ca spikes by FCCP was due to inhibition of oxidative phosphorylation and decrease in ATP, which is necessary for ER Ca-ATPase activity. Finally, the suppression of Ca spikes in Ca free medium suggests that ER Ca storage is replenished via Ca entry from the external medium through store-operated, capacitative Ca entry that may involve certain plasma membrane channels. Overall, these data indicate that ATP triggers Ca release from ER and ER refilling with Ca occur due to capacitive Ca entry into osteocytes from the extracellular matrix.

Purinergic receptors bind to extracellular ATP. Purinergic receptors such as P2X and P2Y have recently been identified in osteocytes, through which extracellular ATP increases $[Ca^{2+}]_c$ (Kringelbach et al., 2015; Zhang et al., 2018). We have previously reported that in mice knockout of P2X7, one of the P2X receptors, associates with a reduced anabolic response to mechanical loading *in vivo* (Li et al., 2005). However, when the Stat3 inhibitor WP1066 was added, ATP-induced increases in $[Ca^{2+}]_c$ were diminished, suggesting that ATP/purinergic receptors-mediated increases in $[Ca^{2+}]_c$ are modulated by Stat3 activity. In astrocytes, extracellular ATP acting at P2X and P2Y receptors stimulates Ser-727 phosphorylation of Stat3 (Washburn and Neary, 2006). Recent data show that Stat3 phosphorylated at Ser-727 can translocate to mitochondria (Wegrzyn et al., 2009; Tammineni et al.,

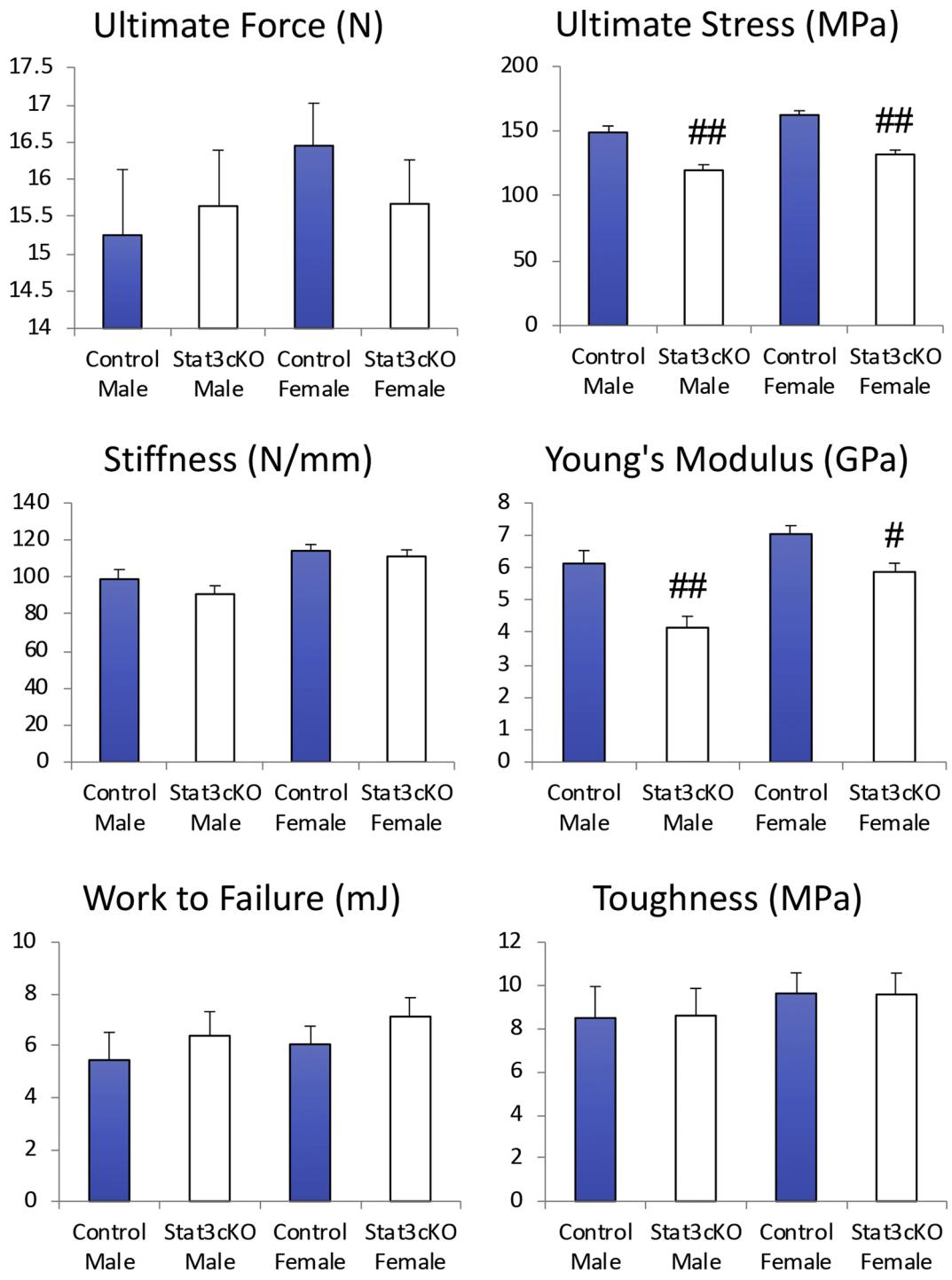

Fig. 4. Stat3 deficiency in osteocytes negatively affects biomechanical properties of cortical bone. The three point bending test of femoral shafts shows that ultimate force, stiffness, and energy to failure were not significantly different between the wild type controls and Dmp1-Cre;Stat3$^{flox/flox}$ (KO) mice. Material properties based on the geometric data measured showed that ultimate stress and Young's modulus were significantly less in Dmp1-Cre;Stat3$^{flox/flox}$ (KO) mice, compared to the wild type controls. Toughness was not different between the wild type controls and Dmp1-Cre;Stat3$^{flox/flox}$ (KO) mice. Note that #: $p < 0.01$ and ##: $p < 0.001$.

2013). It remains to be clarified how Stat3 activation influences $[Ca^{2+}]_c$ in response to extracellular ATP and mechanical loading. It is conceivable that WP1066 inhibits ER refilling with Ca^{2+} either by directly inhibiting Ca^{2+}-ATPase in ER or indirectly via inhibition of Stat3. It is also possible that WP1066 directly or indirectly affects mitochondria and inhibits ATP production, which is necessary for Ca^{2+}-ATPase activity. However, these hypotheses still have to be tested.

The interaction between Stat3 and Wnt signaling pathway may be involved in load induced bone formation. Previous studies have demonstrated that loading increases Wnt target gene expression (Hens et al., 2005; Robinson et al., 2006; Tu et al., 2012). Other studies have shown that SOST/Sclerostin downregulation is required for the increase of bone formation induced by ulnar loading (Robling et al., 2008; Tu et al., 2012). Some similar action patterns between Wnt signaling and Stat3 have been reported. Like Wnt molecules, Stat3 overexpression is found in cancer cells (Klaus and Birchmeier, 2008; Johnson et al., 2018)

Table 1
Geometric properties of osteocyte-specific Stat3 KO mice.

Groups	Total area (mm^2)	Marrow area (mm^2)	Cortical area (mm^2)	Cortical thickness (mm)	AP width (mm)	ML width (mm)	AP to ML Ratio	Cortical area/total area (%)
WT male ($n=6$)	1.660 ± 0.167	0.931 ± 0.124	0.730 ± 0.047	0.185 ± 0.005	1.212 ± 0.077	1.744 ± 0.073	0.695 ± 0.023	44.097 ± 1.834
Stat3 cKO male ($n=8$)	2.009 ± 0.246[a]	1.207 ± 0.156[a]	0.803 ± 0.118	0.182 ± 0.019	1.335 ± 0.094[c]	1.923 ± 0.106[a]	0.694 ± 0.028	39.924 ± 2.757[a]
WT female ($n=14$)	1.548 ± 0.106	0.813 ± 0.094	0.736 ± 0.038	0.195 ± 0.011	1.221 ± 0.052	1.621 ± 0.067	0.755 ± 0.043	47.650 ± 2.779
Stat3 cKO female ($n=13$)	1.716 ± 0.147[a]	0.945 ± 0.083[b]	0.772 ± 0.078	0.192 ± 0.013	1.274 ± 0.052[c]	1.701 ± 0.088[c]	0.750 ± 0.029	44.941 ± 1.919[a]

Data were presented as mean ± S.E.M.
[a] $p < 0.01$ vs. the same sex control.
[b] $p < 0.001$ vs. the same sex control.
[c] $p < 0.05$ vs. the same sex control.

and Stat3 is necessary for self-renewal of stem cells and functions of some differentiated cells, including osteoblasts (Klaus and Birchmeier, 2008; Li, 2013; Galoczova et al., 2018). One study reports that Wnt3a-mediated activation of Stat3 increases the viability of cells exposed to oxidative stress (Fragoso et al., 2012). Our unpublished data shows SOST mRNA is upregulated in Stat3 deficient cells. These data suggest potential cross-talk between Wnt/β-catenin pathway and Stat3 signaling in bone cells, but additional research is needed to elucidate this interaction.

In conclusion, our study has demonstrated that Stat3 signaling in osteocytes is not involved in skeletal development. However, loss-of-function of Stat3 in osteocytes decreases the osteogenic response following mechanical loading. Stat3 deficiency in osteocytes inhibits bone formation and increases bone resorption in adult mice, which leads to a reduction in materials mechanical properties of bone in adult mice. With the knowledge of how Stat3 is involved in the signal transduction through osteocytes and calling other cells into action, novel therapeutic targets for the prevention of osteoporosis can be discovered and, subsequently, new treatments can be developed.

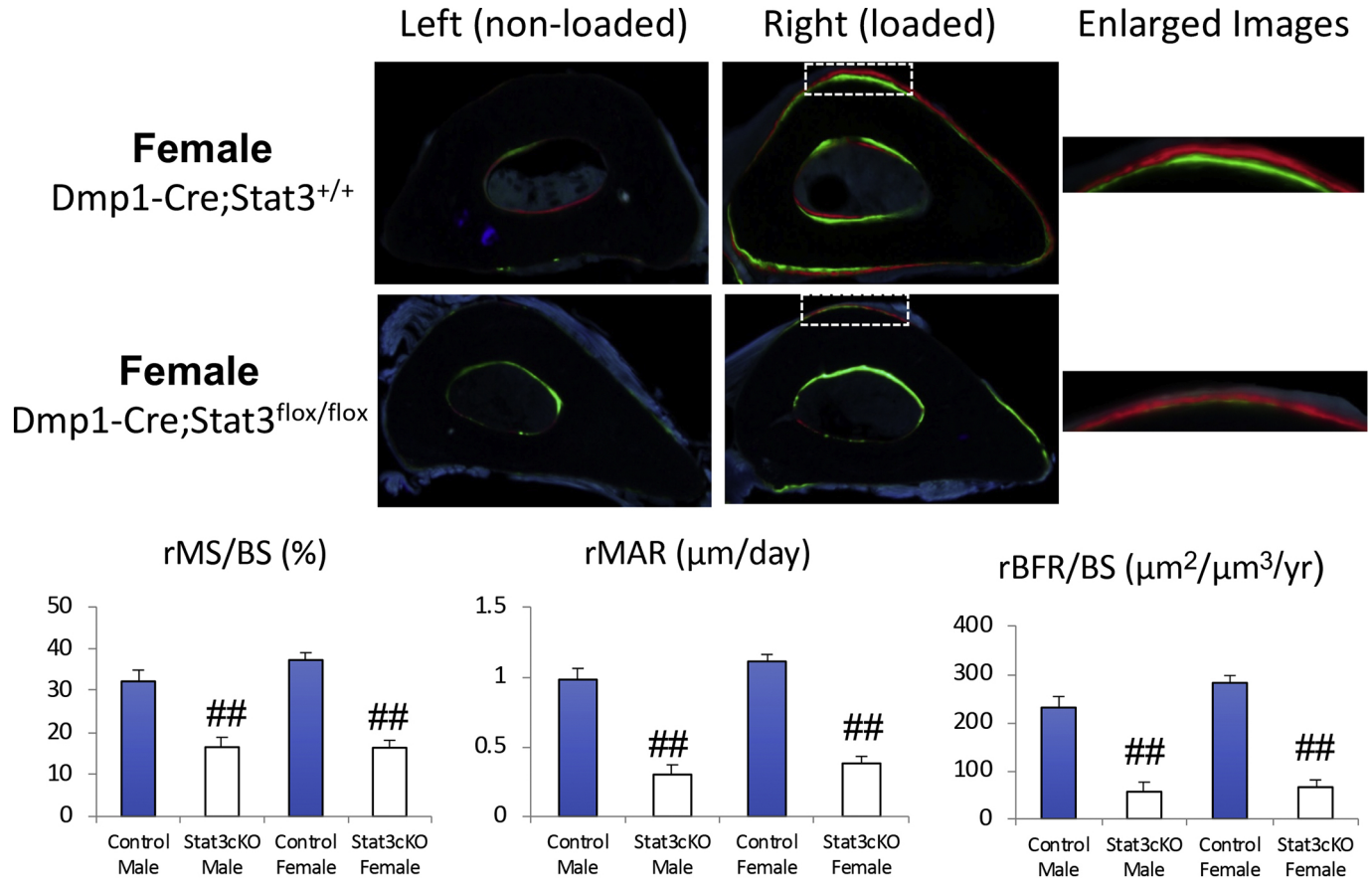

Fig. 5. Stat3 deficiency in osteocytes suppresses mechanically induced bone formation. Midshaft ulnar sections were acquired from the control and loaded forearms for the wild type controls and Dmp1-Cre;$Stat3^{flox/flox}$ (KO) mice. Calcein (green) and alizarin (red) injections were given after loading. Note that the anabolic responses on the medial (square) and lateral surfaces of the loaded control ulna were detected, but those responses were significantly decreased in the loaded ulna of the Dmp1-Cre;$Stat3^{flox/flox}$ (KO) mice. Bone morphometric parameters for the control mice and Dmp1-Cre;$Stat3^{flox/flox}$ (KO) mice include relative mineralizing surface (rMS/BS), relative mineral appositional rate (rMAR) and relative bone formation rate (rBFR/BS). Note that ##: $p < 0.001$.

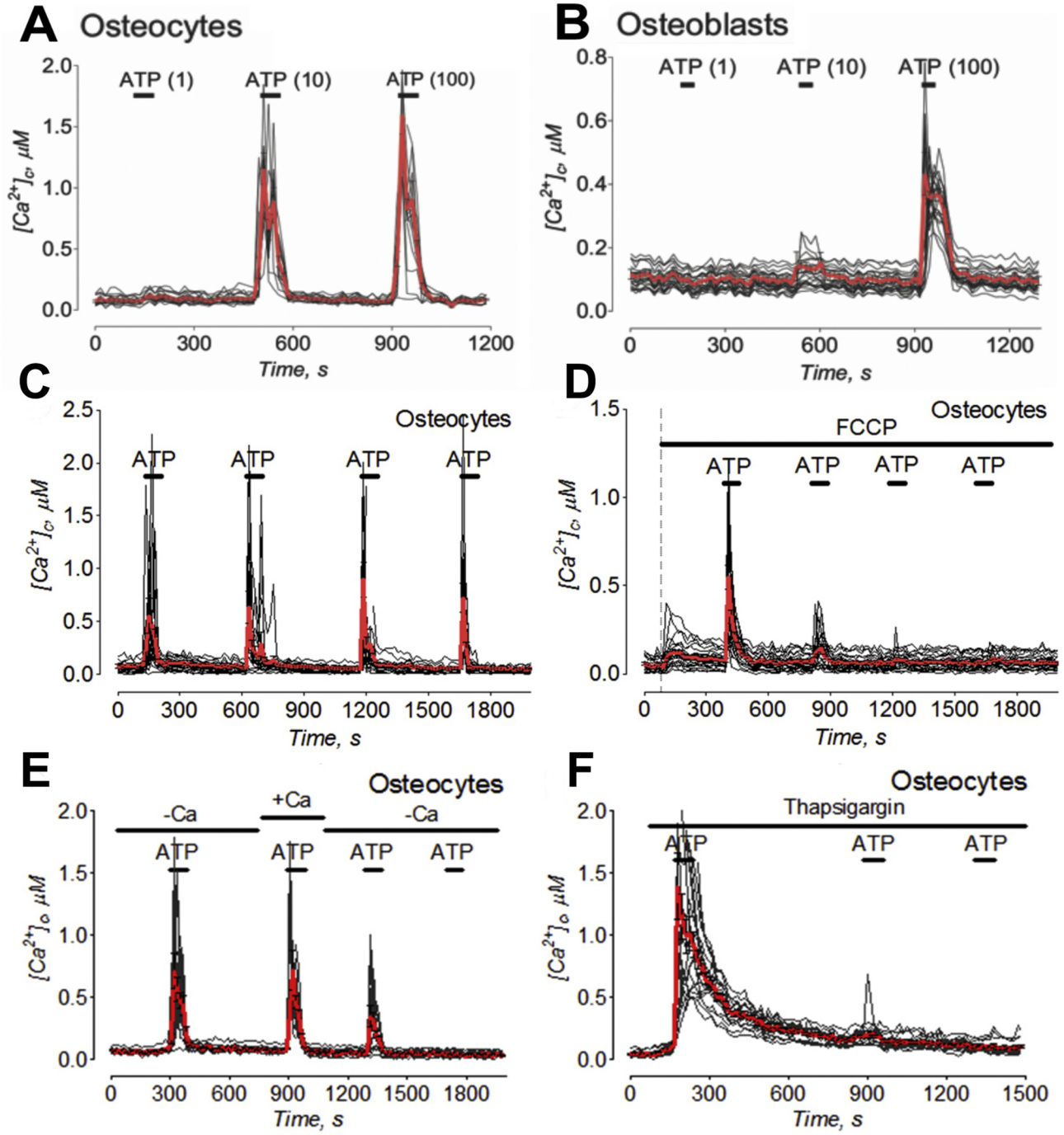

Fig. 6. The effect of external ATP on cytosolic Ca^{2+} concentration ($[Ca^{2+}]_c$) in cultured osteocytes (A, C-F) and osteoblasts (B). In A and B, concentration dependence of ATP-induced Ca^{2+} transients in osteocytes and osteoblasts, respectively. Numbers in parentheses show $CaCl_2$ concentrations in μM. Here, horizontal lines indicate the applied treatment (i.e. ATP application). In C, Ca^{2+} transients in osteocytes triggered by repeated application of external ATP (10 μM, 30 s). In D, 1 μM FCCP inhibited ATP-induced Ca^{2+} transients in osteocytes triggered by 10 μM ATP. Then, ATP was removed by washing cells with ATP-free solution. Fig. 7C shows the dependence of ATP effects on external Ca^{2+}. Where indicated, osteocytes were treated with 10 μM ATP and exposed to 1.8 mM $CaCl_2$ or Ca^{2+}-free solution as indicated. In D, thapsigargin (0.1 μM) inhibited Ca^{2+} transients in osteocytes triggered by 10 μM ATP.

Transparency document

The Transparency document associated with this article can be found, in online version.

Declaration of Competing Interest

The authors declare that there is no conflict of interest.

Acknowledgments

The authors thank Lei Li and Keith Condon for his assistance with tissue collection and processing. This study was supported by the research funds from Biomechanics and Biomaterials Research Center (BBRC), Indiana University-Purdue University Indianapolis (JL), Indiana University Collaborative Research Grant (JL and NB) and National Institutes of Health award R01 NS098772 (NB) and R21 AR074012 (JL).

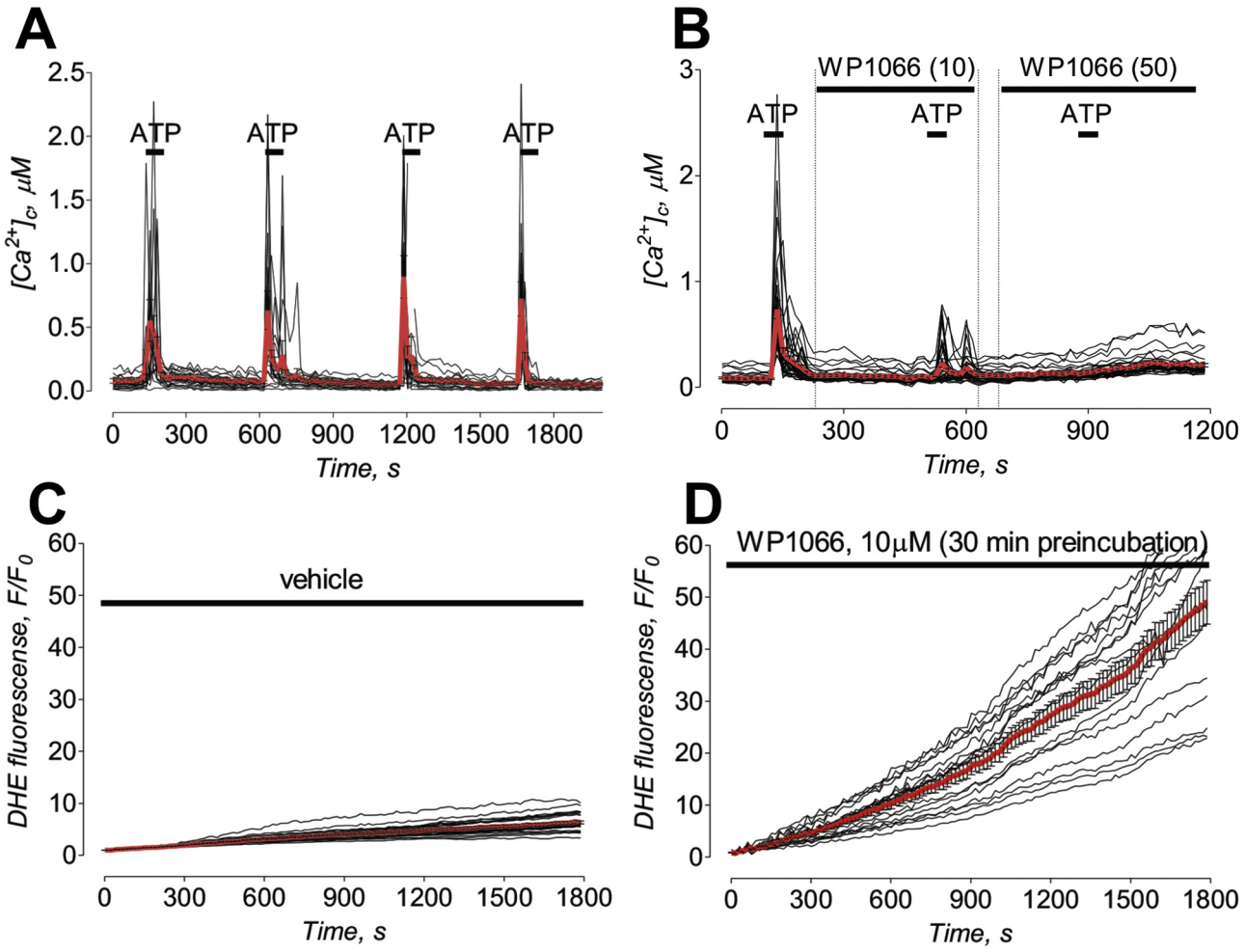

Fig. 7. Inhibition of Stat3 function suppressed cytosolic Ca^{2+} concentration ($[Ca^{2+}]_c$) caused by external ATP and increased ROS production in cultured osteocytes. In A, similar to Fig. 7C, Ca^{2+} transients in osteocytes triggered by repeated application of external ATP (10 μM, 30 s). WP1066, an inhibitor of Stat3, suppressed Ca^{2+} transients triggered by external ATP in osteocytes (B). In B, where indicated, 10 μM ATP, 10 or 50 μM WP1066, were applied to osteocytes. Numbers in parentheses indicate concentrations of the inhibitor in μM. In C, ROS production in vehicle-treated osteocytes. In D, WP1066 increased ROS production in osteocytes. Cells were loaded with dihydroethidium (DHE, 5 μM) and then pre-incubated with a vehicle (0.05% DMSO, E) or 10 μM WP1066 (F) for 30 min. The vehicle (0.05% DMSO) and WP1066 (10 μM) remained in the culture solution during the experiment.

Appendix A. Supplementary data

Supplementary data to this article can be found online at https://doi.org/10.1016/j.bonr.2019.100218.

References

Aaronson, D.S., Horvath, C.M., 2002. A road map for those who don⬢t know JAK-STAT. Science 296 (5573), 1653–1655.

Almeida, M., Han, L., Martin-Millan, M., O⬢Brien, C.A., Manolagas, S.C., 2007. Oxidative stress antagonizes Wnt signaling in osteoblast precursors by diverting beta-catenin from T cell factor- to forkhead box O-mediated transcription. J. Biol. Chem. 282 (37), 27298–27305.

Bakker, A.D., Kulkarni, R.N., Klein-Nulend, J., Lems, W.F., 2014. IL-6 Alters Osteocyte Signaling Toward Osteoblasts but Not Osteoclasts. pp. 394–399.

Berman, A.G., Wallace, J.M., Bart, Z.R., Allen, M.R., 2016. Raloxifene reduces skeletal fractures in an animal model of osteogenesis imperfecta. Matrix Biol. 52–54, 19–28.

Bivi, N., Condon, K.W., Allen, M.R., Farlow, N., Passeri, G., Brun, L.R., Rhee, Y., Bellido, T., Plotkin, L.I., 2012. Cell autonomous requirement of connexin 43 for osteocyte survival: consequences for endocortical resorption and periosteal bone formation. Journal of bone and mineral research: the official journal of the American Society for Bone and Mineral Research 27 (2), 374–389.

Boengler, K., Hilfiker-Kleiner, D., Heusch, G., Schulz, R., 2010. Inhibition of permeability transition pore opening by mitochondrial STAT3 and its role in myocardial ischemia/reperfusion. Basic Res. Cardiol. 105 (6), 771–785.

Chen, N.X., Geist, D.J., Genetos, D.C., Pavalko, F.M., Duncan, R.L., 2003. Fluid shear-induced NFkappaB translocation in osteoblasts is mediated by intracellular calcium release. Bone 33 (3), 399–410.

Dietz, R.M., Kiedrowski, L., Shuttleworth, C.W., 2007. Contribution of Na(+)/Ca(2+) exchange to excessive Ca(2+) loading in dendrites and somata of CA1 neurons in acute slice. Hippocampus 17 (11), 1049–1059.

Fragoso, M.A., Patel, A.K., Nakamura, R.E., Yi, H., Surapaneni, K., Hackam, A.S., 2012. The Wnt/beta-catenin pathway cross-talks with STAT3 signaling to regulate survival of retinal pigment epithelium cells. PLoS One 7 (10), e46892.

Freeman, A.F., Holland, S.M., 2008. The hyper-IgE syndromes. Immunol. Allergy Clin. N. Am. 28 (2), 277–291 (viii).

Galoczova, M., Coates, P., Vojtesek, B., 2018. STAT3, stem cells, cancer stem cells and p63. Cell Mol Biol Lett 23, 12.

Genetos, D.C., Geist, D.J., Liu, D., Donahue, H.J., Duncan, R.L., 2005. Fluid shear-induced ATP secretion mediates prostaglandin release in MC3T3-E1 osteoblasts. Journal of bone and mineral research: the official journal of the American Society for Bone and Mineral Research 20 (1), 41–49.

Genetos, D.C., Kephart, C.J., Zhang, Y., Yellowley, C.E., Donahue, H.J., 2007. Oscillating fluid flow activation of gap junction hemichannels induces ATP release from MLO-Y4 osteocytes. J. Cell. Physiol. 212 (1), 207–214.

Gough, D.J., Corlett, A., Schlessinger, K., Wegrzyn, J., Larner, A.C., Levy, D.E., 2009. Mitochondrial STAT3 supports Ras-dependent oncogenic transformation. Science 324 (5935), 1713–1716.

Grynkiewicz, G., Poenie, M., Tsien, R.Y., 1985. A new generation of Ca2+ indicators with greatly improved fluorescence properties. J. Biol. Chem. 260 (6), 3440–3450.

Hammond, M.A., Laine, T.J., Berman, A.G., Wallace, J.M., 2016. Treadmill exercise improves fracture toughness and indentation modulus without altering the nanoscale morphology of collagen in mice. PLoS One 11 (9), e0163273.

Heinrich, P.C., Behrmann, I., Muller-Newen, G., Schaper, F., Graeve, L., 1998. Interleukin-6-type cytokine signalling through the gp130/Jak/STAT pathway. Biochem. J. 334 (Pt 2), 297–314.

Hens, J.R., Wilson, K.M., Dann, P., Chen, X., Horowitz, M.C., Wysolmerski, J.J., 2005. TOPGAL mice show that the canonical Wnt signaling pathway is active during bone

development and growth and is activated by mechanical loading in vitro. J. Bone Miner. Res. 20 (7), 1103–1113.
Holland, S.M., DeLeo, F.R., Elloumi, H.Z., Hsu, A.P., Uzel, G., Brodsky, N., Freeman, A.F., Demidowich, A., Davis, J., Turner, M.L., Anderson, V.L., Darnell, D.N., Welch, P.A., Kuhns, D.B., Frucht, D.M., Malech, H.L., Gallin, J.I., Kobayashi, S.D., Whitney, A.R., Voyich, J.M., Musser, J.M., Woellner, C., Schaffer, A.A., Puck, J.M., Grimbacher, B., 2007. STAT3 mutations in the hyper-IgE syndrome. N. Engl. J. Med. 357 (16), 1608–1619.
Iwamaru, A., Szymanski, S., Iwado, E., Aoki, H., Yokoyama, T., Fokt, I., Hess, K., Conrad, C., Madden, T., Sawaya, R., Kondo, S., Priebe, W., Kondo, Y., 2007. A novel inhibitor of the STAT3 pathway induces apoptosis in malignant glioma cells both in vitro and in vivo. Oncogene 26 (17), 2435–2444.
Johnson, D.E., O⬢Keefe, R.A., Grandis, J.R., 2018. Targeting the IL-6/JAK/STAT3 signalling axis in cancer. Nat. Rev. Clin. Oncol. 15, 234.
Kido, S., Kuriwaka-Kido, R., Imamura, T., Ito, Y., Inoue, D., Matsumoto, T., 2009. Mechanical stress induces interleukin-11 expression to stimulate osteoblast differentiation. Bone 45 (6), 1125–1132.
Klaus, A., Birchmeier, W., 2008. Wnt signalling and its impact on development and cancer. Nat. Rev. Cancer 8, 387.
Kringelbach, T.M., Aslan, D., Novak, I., Ellegaard, M., Syberg, S., Andersen, C.K., Kristiansen, K.A., Vang, O., Schwarz, P., Jorgensen, N.R., 2015. Fine-tuned ATP signals are acute mediators in osteocyte mechanotransduction. Cell. Signal. 27 (12), 2401–2409.
Levy, D.E., Lee, C.K., 2002. What does Stat3 do? J. Clin. Invest. 109 (9), 1143–1148.
Levy, D.E., Loomis, C.A., 2007. STAT3 signaling and the hyper-IgE syndrome. N. Engl. J. Med. 357 (16), 1655–1658.
Li, J., 2013. JAK-STAT and bone metabolism. JAKSTAT 2 (3), e23930.
Li, J., Liu, D., Ke, H.Z., Duncan, R.L., Turner, C.H., 2005. The P2X7 nucleotide receptor mediates skeletal mechanotransduction. J. Biol. Chem. 280 (52), 42952–42959.
Luvisetto, S., Pietrobon, D., Azzone, G.F., 1987. Uncoupling of oxidative phosphorylation. 1. Protonophoric effects account only partially for uncoupling. Biochemistry 26 (23), 7332–7338.
Mantila Roosa, S.M., Liu, Y., Turner, C.H., 2011. Gene expression patterns in bone following mechanical loading. Journal of bone and mineral research: the official journal of the American Society for Bone and Mineral Research 26 (1), 100–112.
Minegishi, Y., Saito, M., Tsuchiya, S., Tsuge, I., Takada, H., Hara, T., Kawamura, N., Ariga, T., Pasic, S., Stojkovic, O., Metin, A., Karasuyama, H., 2007. Dominant-negative mutations in the DNA-binding domain of STAT3 cause hyper-IgE syndrome. Nature 448 (7157), 1058–1062.
Pellman, J.J., Hamilton, J., Brustovetsky, T., Brustovetsky, N., 2015. Ca(2+) handling in isolated brain mitochondria and cultured neurons derived from the YAC128 mouse model of Huntington⬢s disease. J. Neurochem. 134 (4), 652–667.
Robinson, J.A., Chatterjee-Kishore, M., Yaworsky, P.J., Cullen, D.M., Zhao, W., Li, C., Kharode, Y., Sauter, L., Babij, P., Brown, E.L., Hill, A.A., Akhter, M.P., Johnson, M.L., Recker, R.R., Komm, B.S., Bex, F.J., 2006. Wnt/beta-catenin signaling is a normal physiological response to mechanical loading in bone. J. Biol. Chem. 281 (42), 31720–31728.
Robling, A.G., Hinant, F.M., Burr, D.B., Turner, C.H., 2002. Shorter, more frequent mechanical loading sessions enhance bone mass. Med. Sci. Sports Exerc. 34 (2), 196–202.
Robling, A.G., Niziolek, P.J., Baldridge, L.A., Condon, K.W., Allen, M.R., Alam, I., Mantila, S.M., Gluhak-Heinrich, J., Bellido, T.M., Harris, S.E., Turner, C.H., 2008. Mechanical stimulation of bone in vivo reduces osteocyte expression of Sost/sclerostin. J. Biol. Chem. 283 (9), 5866–5875.
Rubin, C.T., 1984. Skeletal strain and the functional significance of bone architecture. Calcif. Tissue Int. 36 (1), S11–S18.
Sanchez, C., Gabay, O., Salvat, C., Henrotin, Y.E., Berenbaum, F., 2009. Mechanical loading highly increases IL-6 production and decreases OPG expression by osteoblasts. Osteoarthr. Cartil. 17 (4), 473–481.
Sarafian, T.A., Montes, C., Imura, T., Qi, J., Coppola, G., Geschwind, D.H., Sofroniew, M.V., 2010. Disruption of astrocyte STAT3 signaling decreases mitochondrial function and increases oxidative stress in vitro. PLoS One 5 (3), e9532.
Senaldi, G., Varnum, B.C., Sarmiento, U., Starnes, C., Lile, J., Scully, S., Guo, J., Elliott, G., McNinch, J., Shaklee, C.L., Freeman, D., Manu, F., Simonet, W.S., Boone, T., Chang, M.S., 1999. Novel neurotrophin-1/B cell-stimulating factor-3: a cytokine of the IL-6 family. Proc. Natl. Acad. Sci. U. S. A. 96 (20), 11458–11463.
Sowerwine, K.J., Shaw, P.A., Gu, W., Ling, J.C., Collins, M.T., Darnell, D.N., Anderson, V.L., Davis, J., Hsu, A., Welch, P., Puck, J.M., Holland, S.M., Freeman, A.F., 2014. Bone density and fractures in autosomal dominant hyper IgE syndrome. J. Clin. Immunol. 34 (2), 260–264.
Stanika, R.I., Pivovarova, N.B., Brantner, C.A., Watts, C.A., Winters, C.A., Andrews, S.B., 2009. Coupling diverse routes of calcium entry to mitochondrial dysfunction and glutamate excitotoxicity. Proc. Natl. Acad. Sci. U. S. A. 106 (24), 9854–9859.
Tammineni, P., Anugula, C., Mohammed, F., Anjaneyulu, M., Larner, A.C., Sepuri, N.B., 2013. The import of the transcription factor STAT3 into mitochondria depends on GRIM-19, a component of the electron transport chain. J. Biol. Chem. 288 (7), 4723–4732.
Thastrup, O., Cullen, P.J., Drobak, B.K., Hanley, M.R., Dawson, A.P., 1990. Thapsigargin, a tumor promoter, discharges intracellular Ca2+ stores by specific inhibition of the endoplasmic reticulum Ca2(+)-ATPase. Proc. Natl. Acad. Sci. U. S. A. 87 (7), 2466–2470.
Tu, X., Rhee, Y., Condon, K.W., Bivi, N., Allen, M.R., Dwyer, D., Stolina, M., Turner, C.H., Robling, A.G., Plotkin, L.I., Bellido, T., 2012. Sost downregulation and local Wnt signaling are required for the osteogenic response to mechanical loading. Bone 50 (1), 209–217.
Turner, C.H., Forwood, M.R., Otter, M.W., 1994. Mechanotransduction in bone: do bone cells act as sensors of fluid flow? FASEB J. 8 (11), 875–878.
Vergun, O., Sobolevsky, A.I., Yelshansky, M.V., Keelan, J., Khodorov, B.I., Duchen, M.R., 2001. Exploration of the role of reactive oxygen species in glutamate neurotoxicity in rat hippocampal neurones in culture. J. Physiol. 531, 147–163 Pt 1.
Washburn, K.B., Neary, J.T., 2006. P2 purinergic receptors signal to STAT3 in astrocytes: difference in STAT3 responses to P2Y and P2X receptor activation. Neuroscience 142 (2), 411–423.
Wegrzyn, J., Potla, R., Chwae, Y.J., Sepuri, N.B., Zhang, Q., Koeck, T., Derecka, M., Szczepanek, K., Szelag, M., Gornicka, A., Moh, A., Moghaddas, S., Chen, Q., Bobbili, S., Cichy, J., Dulak, J., Baker, D.P., Wolfman, A., Stuehr, D., Hassan, M.O., Fu, X.Y., Avadhani, N., Drake, J.I., Fawcett, P., Lesnefsky, E.J., Larner, A.C., 2009. Function of mitochondrial Stat3 in cellular respiration. Science 323 (5915), 793–797.
Welte, T., Zhang, S.S., Wang, T., Zhang, Z., Hesslein, D.G., Yin, Z., Kano, A., Iwamoto, Y., Li, E., Craft, J.E., Bothwell, A.L., Fikrig, E., Koni, P.A., Flavell, R.A., Fu, X.Y., 2003. STAT3 deletion during hematopoiesis causes Crohn⬢s disease-like pathogenesis and lethality: a critical role of STAT3 in innate immunity. Proc. Natl. Acad. Sci. U. S. A. 100 (4), 1879–1884.
You, J., Jacobs, C.R., Steinberg, T.H., Donahue, H.J., 2002. P2Y purinoceptors are responsible for oscillatory fluid flow-induced intracellular calcium mobilization in osteoblastic cells. J. Biol. Chem. 277 (50), 48724–48729.
Zhang, B., Hou, R., Zou, Z., Luo, T., Zhang, Y., Wang, L., Wang, B., 2018. Mechanically induced autophagy is associated with ATP metabolism and cellular viability in osteocytes in vitro. Redox Biol. 14, 492–498.
Zhou, H., Newnum, A.B., Martin, J.R., Li, P., Nelson, M.T., Moh, A., Fu, X.Y., Yokota, H., Li, J., 2011. Osteoblast/osteocyte-specific inactivation of Stat3 decreases load-driven bone formation and accumulates reactive oxygen species. Bone 49 (3), 404–411.